Biochimica et Biophysica Acta 1797 (2010) 339–346

Contents lists available at ScienceDirect

Biochimica et Biophysica Acta

journal homepage: www.elsevier.com/locate/bbabio

Low-temperature electron transfer suggests two types of Q_A in intact photosystem II

Han Bao, Chunxi Zhang *, Yanan Ren, Jingquan Zhao

Laboratory of Photochemistry, Beijing National Laboratory of Molecular Sciences, Institute of Chemistry, Chinese Academy of Sciences, Beijing 100190, China

ARTICLE INFO

Article history:
Received 5 June 2009
Received in revised form 1 December 2009
Accepted 3 December 2009
Available online 6 January 2010

Keywords:
Photosystem II
Q_A
Tyr_Z
Side-path electron donor
Electron transfer
EPR

ABSTRACT

The correlation between the reduction of Q_A and the oxidation of Tyr_Z or $Car/Chl_Z/Cyt_{b559}$ in spinach PSII enriched membranes induced by visible light at 10 K is studied by using electron paramagnetic resonance spectroscopy. Similar $g = 1.95–1.86$ $Q_A^{-\bullet}$EPR signals are observed in both Mn-depleted and intact samples, and both signals are long lived at low temperatures. The presence of PPBQ significantly diminished the light induced EPR signals from $Q_A^{-\bullet}$, $Car^{+\bullet}/Chl^{+\bullet}$ and oxidized Cyt_{b559}, while enhancing the amplitude of the $S_1Tyr_Z^{\bullet}$ EPR signal in the intact PSII sample. The quantification and stability of the $g = 1.95–1.86$ EPR signal and signals arising from the oxidized Tyr_Z and the side-path electron donors, respectively, indicate that the EPR-detectable $g = 1.95–1.86$ $Q_A^{-\bullet}$ signal is only correlated to reaction centers undergoing oxidation of the side-path electron donors ($Car/Chl_Z/Cyt_{b559}$), but not of Tyr_Z. These results imply that two types of $Q_A^{-\bullet}$ probably exist in the intact PSII sample. The structural difference and possible function of the two types of Q_A are discussed.

1. Introduction

Photosystem II (PSII) is a multi-subunit membrane protein complex that catalyzes the oxidation of water to oxygen and the reduction of plastoquinone (PQ) to plastoquinol (PQH_2) using sunlight [1-3]. The crystal structure of PSII has been reported recently [4-9], and the scheme for the arrangement of the redox cofactors in the PSII reaction center is shown in Fig. 1.

At physiological temperatures, upon light excitation, one electron is released from the primary electron donor (P_{680}) to the primary electron acceptor (Pheo), producing the $P_{680}^{+\bullet}$ and $Pheo^{-\bullet}$ charge pair [10-14]. $Pheo^{-\bullet}$ then delivers the electron to the primary quinone (Q_A) and the secondary quinone acceptor (Q_B) sequentially [15,16]. Meanwhile, $P_{680}^{+\bullet}$ obtains an electron from $Tyr_{D1\text{-}161}$ (Tyr_Z) resulting in a neutral radical, $Tyr_Z^{\bullet}$[17,18], which subsequently drives water oxidation in the Mn-cluster which contains four Mn ions and one Ca^{2+} ion [1,13,19-24].

At liquid helium temperatures (below 77 K), initial charge separation to form $P_{680}^{+\bullet}$ and $Pheo^{-\bullet}$ still takes place [10,13,25,26], while electron transfer from $Q_A^{-\bullet}$ to Q_B is completely blocked [27-29]. $P_{680}^{+\bullet}$ can drive the oxidation of the side-path electron donors ($Car/Chl_Z/Cyt_{b559}$) [30-36] in most PSII preparations, and it can also drive the oxidation of Tyr_Z found recently in intact PSII [37-45]. It was reported recently that the redox properties of non-heme iron and the existence of Q_B significantly affected these secondary electron donors in intact samples [46]. However, the selection mechanism for the oxidation of these secondary electron donors is still unknown. As Q_A is the common electron acceptor for the oxidation of these secondary electron donors, characterization of the formation and stability of the $Q_A^{-\bullet}$ signal would be essential to understand the electron transfer reactions in intact PSII at low temperatures.

Electron paramagnetic resonance (EPR) spectroscopy is one of the most powerful techniques available to characterize the $Q_A^{-\bullet}$ intermediate species [15]. There are different EPR signals reported for $Q_A^{-\bullet}$ in the literature [15,29,47-53]. The $Q_A^{-\bullet}$ EPR signal is usually very weak and broad, and thus difficult to detect and quantify due to the magnetic interaction between $Q_A^{-\bullet}$ and the non-heme iron, Fe^{2+} nearby [15]. Moreover, the g value, spectral shape and the amplitude of the $Q_A^{-\bullet}$ EPR signals are all sensitive to the presence of some anions and/or small molecules (such as, HCO_3^-, CN^-, OH^-, NO, PQ, etc.)[15,29,48-51]. Notably, most of the reported $Q_A^{-\bullet}$ EPR signals were obtained from samples without oxygen-evolving activity, where the low-temperature Tyr_Z oxidation was blocked. So far, the $Q_A^{-\bullet}$ EPR signal corresponding to Tyr_Z oxidation at liquid helium temperatures has only been reported in cyanobacteria PSII core complexes containing the $PQ^{-\bullet}$ at the Q_B position, in which the appearance of the $g = 1.66$ EPR

Abbreviations: Chl, chlorophyll; Chl_Z, side-path redox active Chl; Car, redox active β-carotene; Cyt_{b559}, cytochrome b559; D1, D2, reaction center core proteins; DMSO, dimethyl sulfoxide; EDTA, ethylenediaminetetraacetic acid; EPR, electron paramagnetic resonance; MES, 4-morpholine ethanesulfonic acid; P_{680}, primary electron donor of PSII; P_{D1}, P_{D2}, two monomeric Chls of P_{680} associated with D_1 and D_2, respectively; Pheo, pheophytin; PPBQ, phenyl-*p*-benzoquinone; PSII, photosystem II; PQ, plastoquinone; PQH_2, plastoquinol; Q_A and Q_B, primary and secondary quinone electron acceptors, respectively; Tyr_D, tyrosine 161 of the D_1 protein; Tyr_Z, tyrosine 160 of the D_2 protein

* Corresponding author. Tel.: +86 10 82617053; fax: +86 10 82617315.
E-mail address: chunxizhang@iccas.ac.cn (C. Zhang).

0005-2728/$ – see front matter © 2009 Elsevier B.V. All rights reserved.
doi:10.1016/j.bbabio.2009.12.001

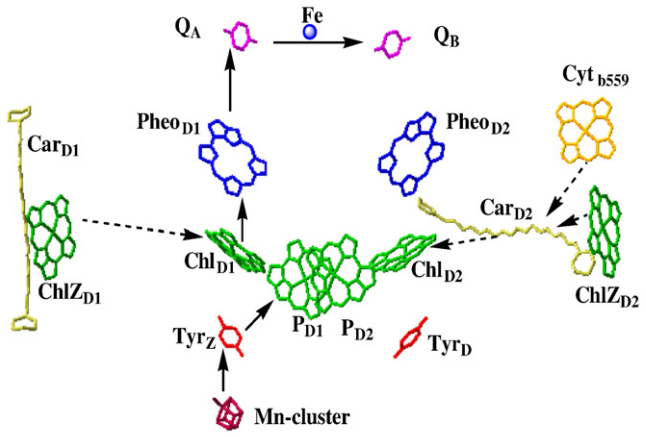

Fig. 1. Scheme for the redox cofactors in the PSII reaction center.

signal arising from $Q_A^{-\bullet}Fe^{2+}Q_B^{-\bullet}$ was found to correlate to the Tyr_Z oxidation [40]. In spinach PSII, the $g=1.66$ $Q_A^{-\bullet}Fe^{2+}Q_B^{-\bullet}$ EPR signal was not observable due to the lack of PQ molecule at the Q_B position. It was also reported that a $g=1.87$ EPR signal correlated with Tyr_Z as well [40]. However, we notice that the assignment of the $g=1.87$ signal to $Q_A^{-\bullet}Fe^{2+}$ suffered from overlap with the EPR signals of the $S_1Tyr_Z^{\bullet}$, and the co-existence of some fraction of $S_0Tyr_Z^{\bullet}$ induced at liquid helium temperatures. Therefore, correlation of Q_A reduction to the oxidation of the secondary electron transfers at low temperature in intact PSII, especially, in the widely used spinach PSII samples, is still an open question.

Here, we use EPR spectroscopy to monitor the reduction of Q_A and the oxidation of Tyr_Z or the side-path electron donors (Car/Chl_Z/Cyt_{b559}), respectively, from spinach PSII induced by visible light at liquid helium temperatures. Our results indicate that two types of $Q_A^{-\bullet}$ probably exist in intact spinach PSII, which determines the oxidation of the secondary electron donors at low temperatures.

2. Materials and methods

PSII enriched membranes were isolated from spinach following the method of Berthold et al. [54] with modifications as described in ref [46]. The final PSII membranes were suspended in a buffer containing 400 mM sucrose, 15 mM NaCl, 5 mM $MgCl_2$, 5 mM $CaCl_2$, 25 mM MES/NaOH, (pH = 6.5), and were frozen in liquid nitrogen and stored at −80 °C until use. Typical oxygen evolving rates were 600 ~ 800 μmol O_2 (mg Chl)$^{-1}$ h^{-1}, measured with a Clark-type electrode at 25 °C in the presence of 0.3 mM PPBQ.

Mn-depleted PSII was obtained by using NH_2OH and EDTA treatment as described in ref [32]. Mn ions and NH_2OH were removed by washing with a buffer containing 400 mM sucrose, 15 mM NaCl, 5 mM $MgCl_2$, 2 mM EDTA, 25 mM MES/NaOH (pH = 6.5) five times, then washed with the same buffer with 0.5 mM EDTA. The final Mn-depleted samples were frozen in liquid nitrogen and stored at −80 °C until use.

EPR samples for PSII enriched membranes were prepared according to ref [46]. Briefly, PSII enriched membranes were thawed and washed with a buffer containing 400 mM sucrose, 15 mM NaCl, 10 mM $CaCl_2$, 1 mM EDTA, and 25 mM MES/NaOH (pH = 6.5). The pellet was dissolved into the same buffer to a Chl concentration of 1 mg/ml, then exposed to room-light at 0 °C for 2 min. The samples were washed once more, and re-suspended into the same buffer without EDTA, then the sample was transferred into EPR tubes. After to h of dark adaptation at 0 °C, PPBQ from a fresh 20 mM solution in DMSO or methanol was added to a final concentration of 1 mM. After addition of PPBQ, the sample was frozen, first in dry ice/ethanol, then in liquid nitrogen. The final Chl concentration of the EPR samples was about 10 mg Chl/ml.

EPR samples for Mn-depleted PSII were prepared as follows. The Mn-depleted samples were diluted with a buffer containing 400 mM sucrose, 15 mM NaCl, 25 mM MES/NaOH, (pH = 6.5) to an 0.5 mg/mL of Chl concentration, and exposed to room light for 1 min at 0 °C in the presence of 0.5 mM $K_3Fe(CN)_6$. The sample was washed with a buffer containing 400 mM sucrose, 15 mM NaCl, 5 mM $MgCl_2$, 25 mM MES/NaOH, (pH = 6.5) twice, and resuspended into the same buffer, and transferred into EPR tubes. PPBQ from a fresh 20 mM solution in DMSO was added to a final concentration of 1 mM. After addition of PPBQ, the sample was frozen, first in dry ice/ethanol, then in liquid nitrogen. The final Chl concentration of the EPR samples was about 10 mg Chl/ml.

Low-temperature continuous wave EPR spectra and kinetics were recorded on a Bruker E500 spectrometer equipped with an Oxford ESR 900 liquid helium cryostat and ITC-503 temperature controller. A super-high sensitivity resonance cavity (4122SHQE) with a rectangular window was used for all measurements. Before EPR measurements, all samples were degassed with nitrogen gas at 200 K as described in a previous report [55]. Continuous visible light illumination at liquid helium temperature was carried out directly in the EPR cavity as described in ref [46,55,56]. EPR spectrometer settings are given in the figure legends.

3. Results

The $Q_A^{-\bullet}$ EPR signal from PSII is usually broad and weak due to magnetic interaction with the non-heme Fe^{2+} [15], and thus difficult to detect. In most previous reports, the $Q_A^{-\bullet}$ EPR signals were observed at very low temperatures (4–5 K) and high microwave power (20–100 mW). Under these conditions, the different microwave power saturation behaviors of other paramagnetic species (such as, the Mn-cluster, Cyt_{b559}, etc.) make the $Q_A^{-\bullet}$ signal less observable and unquantifiable. In our experiment, a super-high sensitivity resonance cavity was used to obtain a much higher signal-to-noise ratio than the standard resonance cavity used in most previous reports to measure the $Q_A^{-\bullet}$ EPR signals. Therefore, we observed $Q_A^{-\bullet}$ EPR signals at relatively higher temperature (10 K) and lower microwave power (1 mW).

3.1 Formation of $Q_A^{-\bullet}$ and $Car^{+\bullet}/Chl_Z^{+\bullet}$ EPR signals in Mn-depleted samples

Fig. 2A shows the EPR spectrum induced by visible light illumination on the Mn-depleted sample at 10 K. A $g=1.95$–1.86 EPR signal is clearly resolved, which has been assigned to the $Q_A^{-\bullet}$ EPR signals [39,46,49]. Corresponding to the formation of $Q_A^{-\bullet}$ at the acceptor site, there should be oxidation of electron donors at the donor site. In PSII, the possible candidate electron donors include Tyr_Z, Tyr_D, Cyt_{b559} and Car/Chl_Z. However, the oxidation of $TyrB_{ZB}$ is known to be completely blocked in Mn-depleted PSII [38,57,58], and Tyr_D is fully oxidized in the Mn-depleted sample. Cyt_{b559} was also fully pre-oxidized by $K_3Fe(CN)_6$ in our experiment (see Materials and methods for details). Accordingly, the contribution to the $Q_A^{-\bullet}$ EPR signal in Fig. 2A from Tyr_Z, Tyr_D and Cyt_{b559} can be safely ruled out. The sole possible electron donor is Car/Chl_Z. Fig. 2B shows a narrow (10 G, $g=2.00$) EPR signal formed simultaneously with the $Q_A^{-\bullet}$ signal during light illumination. This signal is well known to be assigned to $Car^{+\bullet}/Chl_Z^{+\bullet}$ [34].

Fig. 2C shows decay kinetics of $Q_A^{-\bullet}$ (curve a) and $Car^{+\bullet}/Chl_Z^{+\bullet}$ (curve b) signals at 10 K in the dark. Decay kinetics of the $Q_A^{-\bullet}$ (curve a) and $Car^{+\bullet}/Chl_Z^{+\bullet}$ (curve b) EPR signals are essentially the same, with only a decrease of 20% of the amplitude after 30 min of darkness. Therefore, the fraction of reaction centers undergoing Q_A reduction to give the $g=1.95$–1.86 signal (Fig. 2A) should be equal

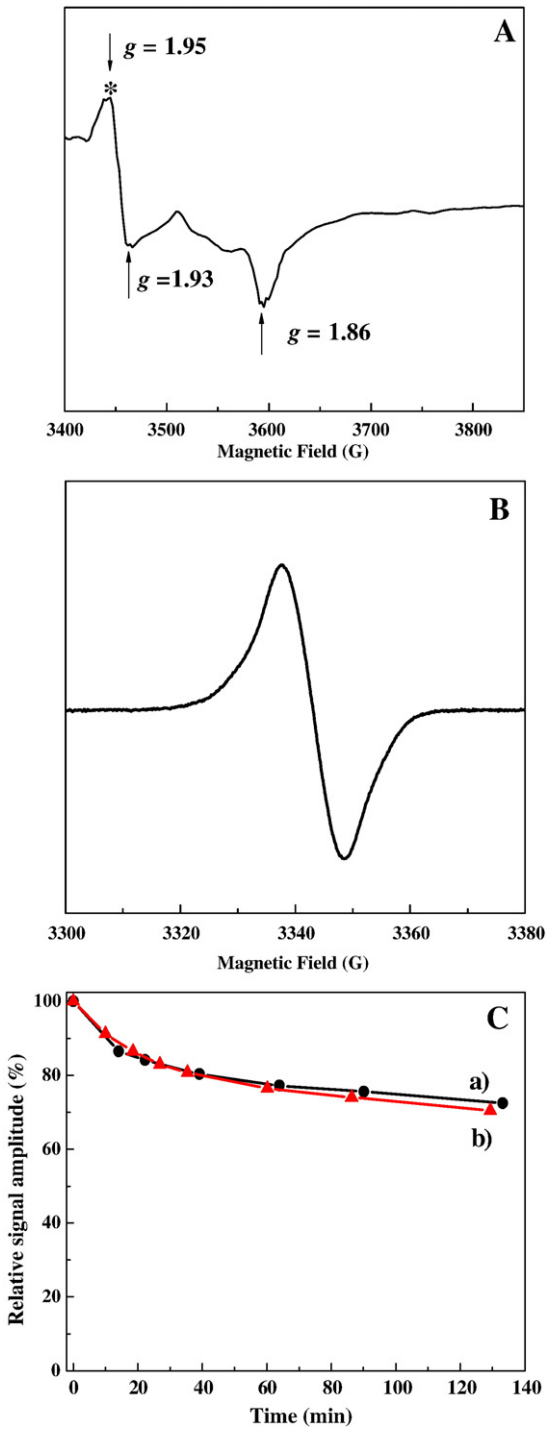

Fig. 2. EPR spectra of $Q_A^{-\cdot}$ (A) and $Car^{+\cdot}/Chl_Z^{+\cdot}$ (B) induced by visible light from Mn-depleted samples at 10 K. The spectrum was obtained by subtracting the spectrum recorded before illumination from that recorded during illumination. EPR conditions for spectrum in panel A: temperature, 10 K; microwave power, 1 mW; modulation amplitude, 18 G; modulation frequency, 100 kH_Z. EPR conditions for spectrum in panel B: microwave power, 5 μW; modulation amplitude, 4 G; other conditions were the same as in panel A. (C) Time-dependency of $Q_A^{-\cdot}$ (curve a, black) and $Car^{+\cdot}/Chl_Z^{+\cdot}$ (curve b, red) EPR signals in the dark at 10 K. For clarity, the maximum amplitudes for both signals are normalized to 100%.

to that of Car/Chl_Z oxidation (Fig. 2B). Quantification of the latter can be performed by comparing the double-integrated area of the $Car^{+\bullet}/Chl_Z^{+\bullet}$ EPR signal (Fig. 2B) to the full $Tyr_D^{\bullet}$ EPR signal (data not shown). We estimate that the $g = 1.95–1.86$ $Q_A^{-\bullet}$ EPR signal in Fig. 2A arises from about 25% of the reaction centers in the Mn-depleted sample.

3.2 Oxidation of Tyr_Z, Car/Chl_Z and Cyt_{b559} in intact PSII

The spectra in Fig. 3A–C show the oxidations of Tyr_Z and the side-path electron donors induced by visible light illumination at 10 K in intact PSII. The spectrum presented as a solid line in Fig. 3A shows a $g = 2.03$ EPR signal from the sample containing PPBQ. This signal was assigned to $S_1Tyr_Z^{\bullet}$ [38-41,46], which decays quickly in the dark with a half-life time of about 3 min (see below Fig. 4 curve a). In

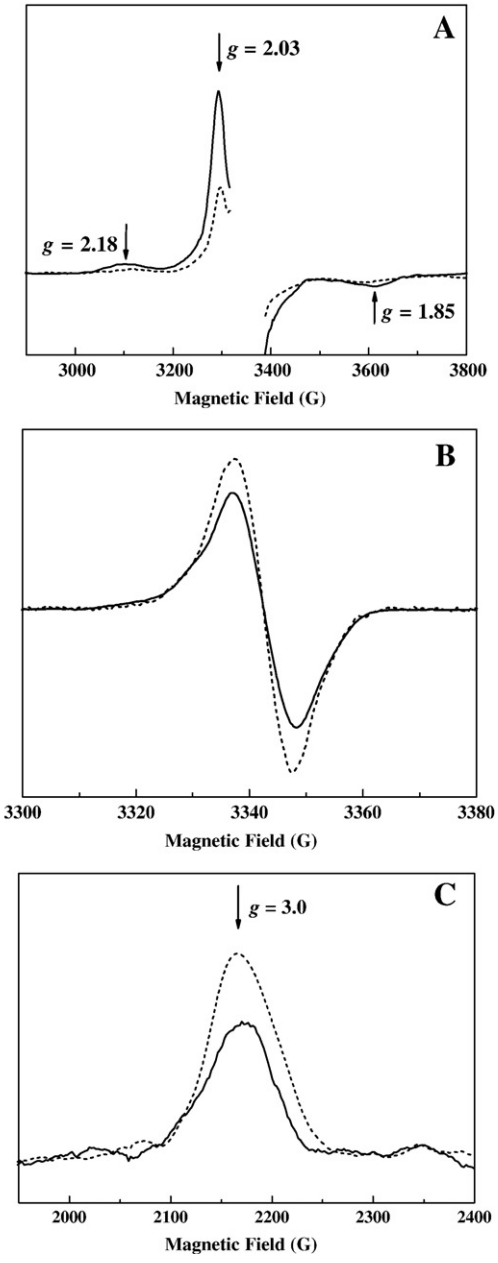

Fig. 3. EPR signals of $S_1Tyr_Z^{\bullet}$ (A), $Car^{+\cdot}/Chl_Z^{+\cdot}$ (B) and g_z of Cyt_{b559} (C) in intact PSII samples at 10 K, with PPBQ present (solid line) and without PPBQ (dashed line). EPR conditions for panel (A) and (C) were the same as in Fig. 2 A; EPR conditions for panel (B) were the same as in Fig. 2B. The spectra in panel A were obtained by subtracting the spectrum recorded 30 min after illumination in the dark from the spectrum recorded during illumination. The spectra in panels B and C were obtained by subtracting the spectrum recorded before illumination from the spectrum recorded immediately after illumination in the dark. For clarity, the Tyr_D signal in the middle of the spectrum in panel A was deleted.

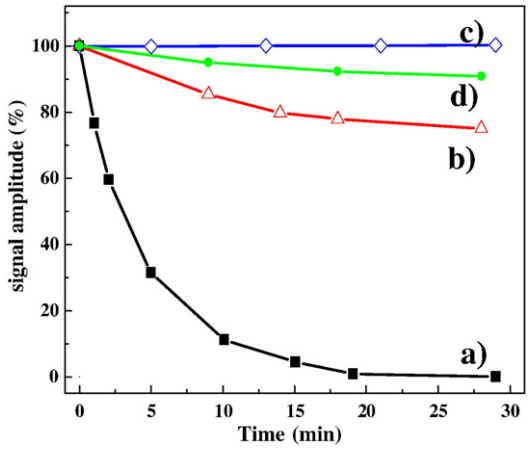

Fig. 4. Time-dependency of $S_1Tyr_Z^{\bullet}$ (curve a, black), $Car^{+\cdot}/Chl_Z^{+\cdot}$ (curve b, red) and $Cyt_{b559(ox)}$ (curve c, blue) and $Q_A^{-\cdot}$ (curve d, green) EPR signals after visible light illumination recorded in intact PSII samples in the presence of PPBQ at 10 K in the dark. The data points were taken by using the amplitude at $g=2.03$ for $S_1Tyr_Z^{\bullet}$ EPR signal (Fig. 3A), at 3337 G position for $Car^{+\cdot}/Chl_Z^{+\cdot}$ signal, the $g_z=3.08$ for oxidized Cyt_{b559} signal (Fig. 3C), the $g=1.9$ for $Q_A^{-\cdot}$ signal with different time delays. Curve d was obtained from the sample containing 6% methanol; curves a, b and c were obtained from the samples without methanol. For clarity, the amplitudes for all signals were normalized to 100%.

addition, due to the high signal-to-noise ratio of the super-high sensitivity resonance cavity used, the satellite peaks of the $S_1Tyr_Z^{\bullet}$ signal at $g=2.18$ and 1.85 is clearly observable [55]. The spectrum presented as a dashed line in Fig. 3A shows the $S_1Tyr_Z^{\bullet}$ signal induced from the sample without PPBQ. The amplitude of the $g=2.03$ signal in the sample without PPBQ (spectrum in dashed line) is decrease to 45% of that in the sample with PPBQ (spectrum in solid line). According to the method of the quantification of Tyr_Z oxidation in previous report [46], we could infer that the fraction of reaction centers undertaking the Tyr_Z oxidation increases about 25% upon the addition of PPBQ at 10K.

The oxidations of the side-path electron donors (Car/Chl_Z and Cyt_{b559}) in the dark-adapted sample containing PPBQ are shown as the solid lines in Fig. 3B and C. The $Car^{+\bullet}/Chl_Z^{+\bullet}$ narrow signal ($g=2.00$) in Fig. 3B shown as a solid line is quantified by using a method similar to that described above in the Mn-depleted sample, and we estimate that the signal arises from 20%–25% of the total reaction centers. The g signal of Cyt_{b559} in Fig. 3C (solid line) is also quantified by comparing the signal with that in Mn-depleted sample in which all Cyt_{b559} was in the oxidized state. The signal in Fig. 3C arises from 30%–35% reaction centers in the sample. Accordingly, the total fraction of reaction centers undergoing the side-pathway is about 50–60%, and the remaining 40–50% should correspond to the fraction of reaction centers undergoing the Tyr_Z oxidation. It should be pointed out that the yield for the oxidation of both the side-path electron donors and Tyr_Z found here are consistent with previous reports [40,46].

The light induced $Car^{+\bullet}/Chl_Z^{+\bullet}$ and oxidized Cyt_{b559} signals from intact sample without PPBQ are shown as the spectra in dashed lines in Fig. 3B and C. Interestingly, the amplitudes of both the $Car^{+\bullet}/Chl_Z^{+\bullet}$ and the g signal of Cyt_{b559} induced by light from the intact sample without PPBQ are significantly higher than those in the samples with PPBQ, which implies that the presence of PPBQ suppresses the side-pathway reactions. The PPBQ effect on the oxidation of the side-path electron donors (Fig. 3B and C) is in sharp contrast to the enhancement effect on Tyr_Z oxidation (in Fig. 3A and ref [46]). The opposite PPBQ dependence of the two types of reactions indicates that the reaction centers participating in the oxidation of the side-path electron donors may be converted into reaction centers conducting Tyr_Z oxidation upon the addition of external quinone in intact PSII.

The stabilities of the light induced $Car^{+\bullet}/Chl_Z^{+\bullet}$ and oxidized Cyt_{b559} signal are shown in Fig. 4 curve b and c, respectively. In contrast to the fast decay of the $S_1Tyr_Z^{\bullet}$ signal (Fig. 4, curve a), both the oxidized Cyt_{b559} and $Car^{+\bullet}/Chl_Z^{+\bullet}$ signals induced by visible light are very stable at 10 K. There is no any observable decay in 30 min of darkness for the former (Fig. 4, curve c), and only about 25% of the total amplitude of the $Car^{+\bullet}/Chl_Z^{+\bullet}$ signal diminishes after half an hour in the dark (see Fig. 4 curve b). It should be pointed out that the decay fraction of $Car^{+\bullet}/Chl_Z^{+\bullet}$ signal in 30 min of darkness corresponds to only about 5% of the total reaction centers in the sample.

3.3. Reduction of Q_A in intact PSII

It is known that most $Q_A^{-\bullet}$ EPR signals have absorption in the $g=2.0$–1.8 range, which obviously overlaps with the $S_1Tyr_Z^{\bullet}$ signal. To avoid the contribution of $S_1Tyr_Z^{\bullet}$ to the possible $Q_A^{-\bullet}$ EPR signal, we measured the $Q_A^{-\bullet}$ signal in the intact sample containing 6% methanol because the presence of methanol was reported to remove the $S_1Tyr_Z^{\bullet}$ signal [59,60], but to leave the $Q_A^{-\bullet}$ EPR signal unchanged [55]. Indeed, we find that the peaks at $g=2.03$, 2.18 and 1.85 due to the $S_1Tyr_Z^{\bullet}$ signal (in Fig. 3A) all completely disappeared after addition of 6% methanol to the sample, while the $g=1.95$–1.86 $Q_A^{-\bullet}$ EPR signal is clearly observed as shown in Fig. 5A. Moreover, this $Q_A^{-\bullet}$ signal is long lived as well, and only about 10% of the amplitude decays in half an hour (as shown in Fig. 4 curve d), which is clearly different from the faster decay of the $S_1Tyr_Z^{\bullet}$ signal (Fig. 4 curve a). Considering the

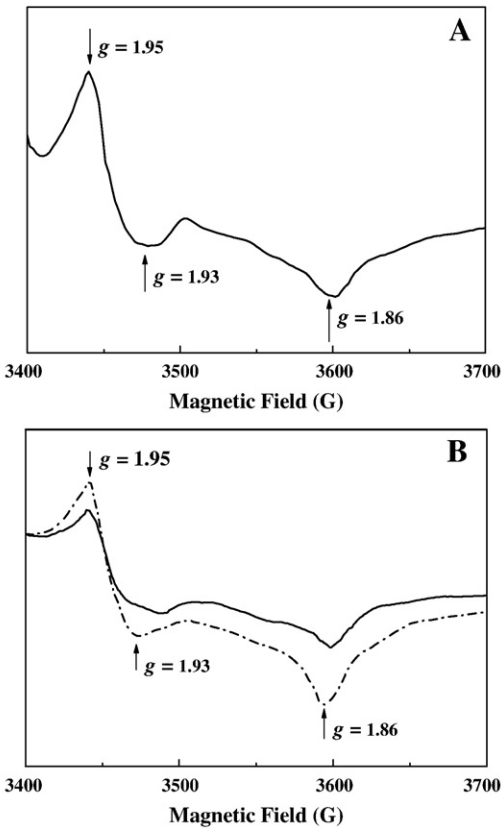

Fig. 5. EPR signals of $Q_A^{-\cdot}$ in intact PSII samples induced at 10 K. The spectrum in panel A was obtained by subtracting the spectrum recorded before illumination from that recorded immediately after illumination from the sample containing 6% methanol and 1 mM PPBQ. Spectra in panel B were obtained by subtracting the spectrum recorded before illumination from that recorded 30 min after illumination in the dark from the sample with PPBQ present (solid line) and without (dashed line). EPR conditions were the same as in Fig. 2 A.

similar spectral shape and g value of the $Q_A^{-\bullet}$ signal in both Mn-depleted and intact PSII, we have quantified the $g=1.95$–1.84 EPR signal in intact sample (Fig. 5A) by comparing the signal with that in Mn-depleted samples, and estimate that the $Q_A^{-\bullet}$ signal (Fig. 5A) arises from 50% to 60% of the reaction centers, and thus the decay fraction of this signal in half an hour correlates to ~5% of the reaction centers. It is worth pointing out that the decay fraction of the $Q_A^{-\bullet}$ signal is nearly equal to that of the $Car^{+\bullet}/Chl_Z^{+\bullet}$ radical described above, which strongly implies that the decay fraction of the $Q_A^{-\bullet}$ signal is probably correlated to the decay of the $Car^{+\bullet}/Chl_Z^{+\bullet}$ signal. In addition, the 50–60% fraction of reaction centers which undergo the side-pathway is nearly the same as the fraction of reaction centers in the state $Q_A^{-\bullet}$. These results indicate that $Q_A^{-\bullet}$ may only associate with the side-path reactions, and the decay fraction is related to that of $Car^{+\bullet}/Chl_Z^{+\bullet}$. Obviously, the stable fraction of $Q_A^{-\bullet}$ is associated with the stable oxidized Cty_{b559} and some stable fraction of $Car^{+\bullet}/Chl_Z^{+\bullet}$. The similarities in the quantification and dynamics of the $Q_A^{-\bullet}$ and the oxidized Car/Chl_Z and Cyt_{b559} strongly suggest that the observed $Q_A^{-\bullet}$ signal may only correlate with the oxidation of the side-path electron donor.

The $Q_A^{-\bullet}$ signal described above in the sample containing methanol was observed also in the sample without methanol as shown in Fig. 5B. The spectrum shown as a solid line was obtained by subtracting the spectrum recorded before illumination from the spectrum recorded 30 min after illumination in the dark. We emphasize that any contribution from $S_1Tyr_Z^{\bullet}$ to this spectrum in Fig. 5 can be safely ruled out as the $S_1Tyr_Z^{\bullet}$ signal decays rapidly, and completely disappears after 30 min of darkness. Interestingly, the $g=1.95$–1.86 EPR signal is significantly increased in the absence of PPBQ (see Fig. 5B). One may argue that the decrease of the $Q_A^{-\bullet}$ EPR signal in the sample with PPBQ could be due to the presence of Fe^{3+} formed after the oxidation of non-heme iron by $PPBQ^{-\bullet}$ [61]. The contribution of Fe^{3+} to the decrease in the $Q_A^{-\bullet}$ EPR signal can be verified by monitoring the change in the Fe^{3+} signal ($g=8.0$–5.0) in the sample during and after illumination at 10 K. We did not observe any change in the $g=8.0$–5.0 range during and after 10 K illumination (data not shown). Thus, the Fe^{3+} species does not contribute to the decrease of the $g=1.95$–1.86 signal in the sample containing PPBQ.

In contrast to the enhancement effect on the $S_1Tyr_Z^{\bullet}$ signal (in Fig. 3A), the presence of PPBQ decreases the amplitude of the $g=1.95$–1.86 EPR signal (in Fig. 5B), which is similar to the suppression effect on oxidation of the side-path electron donors (Fig. 3B and C). The different PPBQ effects on $S_1Tyr_Z^{\bullet}$ and $Q_A^{-\bullet}$ add further support that the observed $g=1.95$–1.86 $Q_A^{-\bullet}$ signal is only correlated to the oxidation of the side-path electron donors, but not of Tyr_Z in intact PSII.

4. Discussion

4.1. Two types of Q_A in intact PSII from spinach

Our results on the relationship between Q_A reduction and the oxidation of Tyr_Z or $Car/Chl_Z/Cyt_{b559}$ in spinach PSII enriched membranes indicates that two types of $Q_A^{-\bullet}$ probably exist in intact PSII. One is correlated with the reaction centers undergoing the side-path electron donors oxidation to give rise to the observed $g=1.95$–1.86 $Q_A^{-\bullet}$ EPR signal. The other is correlated with the reaction centers, where Tyr_Z oxidation occurs and the corresponding $Q_A^{-\bullet}$ EPR signal could be too broad to be detected using X-band EPR. It should be pointed out that these two types of $Q_A^{-\bullet}$ are observed in intact PSII with full oxygen-evolving ability (600–800 μmol O_2 (mg Chl)$^{-1}$ h^{-1}). This differs from various $Q_A^{-\bullet}$ EPR signals reported previously in the literature, where the samples had no or very low water oxidation activity due to various treatment conditions, for example, H^+, OH^-, formate, CN^-, NO, etc. To our knowledge, this is the first time to show that two types of Q_A probably exist in the intact PSII samples with full oxygen-evolving ability. It is noted that two types of Q_A has been also suggested recently in the purple bacteria reaction center [62]. In addition, the two types of Q_A in PSII suggested here can explain the observation of the strong correlation between the effects on the recombination rate and on thermoluminescence reported recently [63].

The $Q_A^{-\bullet}$ EPR signal is known to arise from the magnetic interaction between $Q_A^{-\bullet}$ and the non-heme iron Fe^{2+}[15,64,65]. In PSII, the D_2-His_{214} residue links Q_A and $Fe^{2+}$by forming a hydrogen bond with Q_A and a coordination bond with Fe^{2+}. It is very likely that the strength of the H-bond could significantly affect the spin-spin exchange interaction between $Q_A^{-\bullet}$ and Fe^{2+}, and it can be predicted that the strong and weak exchange coupling would associate with the presence of strong and weak hydrogen bonds between Q_A and His_{214}, respectively. Furthermore, it is known that the width of the EPR signal is strongly dependent on the exchange coupling between two paramagnetic spin species, and the EPR signal becomes narrow when the exchange coupling becomes stronger [65,66]. Since similar $g=1.95$–1.86 $Q_A^{-\bullet}$ EPR signals are observed in the reaction centers of Mn-depleted sample and the fraction undertaking the oxidation of side-path electron donors in intact PSII samples (Fig. 2A and Fig. 5), one can deduce that similar exchange interactions between $Q_A^{-\bullet}$ and Fe^{2+} probably are present in these reaction centers. As FTIR studies [67-69] have shown that the strength of the hydrogen-bond between $Q_A^{-\bullet}$ and D_2-His_{214} in the Mn-depleted sample is strong, we suggest that a similar strong hydrogen-bond probably is present in the reaction centers undergoing oxidation of the side-path electron donors in intact PSII (see Fig. 6 Type 2). In contrast, the strength of the hydrogen bond could be weak in the reaction centers undergoing

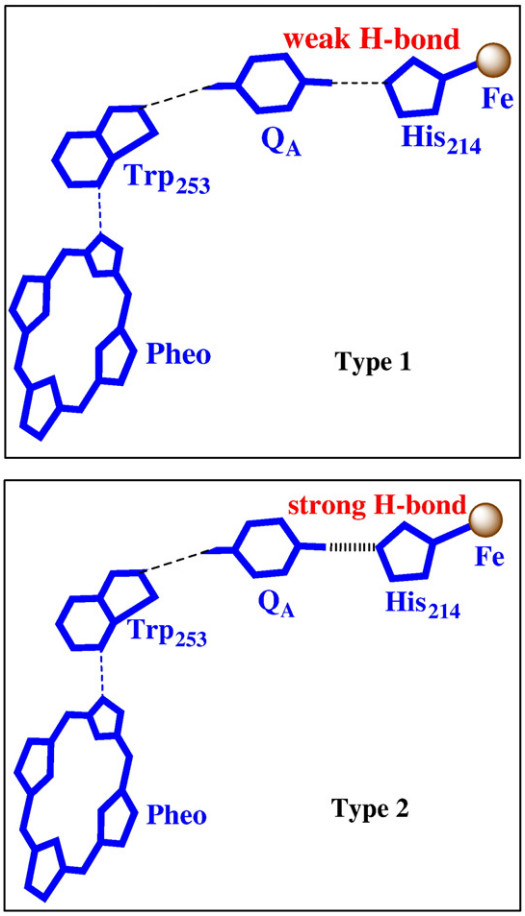

Fig. 6. Scheme for the interaction between Pheo and Q_A in the two types of reaction centers.

Tyr_Z oxidation (see Fig. 6 Type 1), so that the possible $Q_A^{-\bullet}$ EPR signal is probably too broad to be detected due to the weak exchange narrow effect [66]. It is noted that the hydrogen-bond strength between Q_A and His_{214} is still not unambiguously known due to the low resolution of the structural data and the X-ray radiation damage observed recently [70-72]. However, the above prediction of two types of Q_A is also supported by the finding of two midpoint forms of Q_A reported by Johnson et al. [73]. It is expected that the Q_A with the strong hydrogen bond would have a higher redox potential than that with the weak hydrogen bond in intact PSII, as higher stabilization energy would be provided by the strong hydrogen bond than by the weak one.

4.2. Possible physiological functions of the two configurations of Q_A

The PPBQ dependence of the observed $Q_A^{-\bullet}$ EPR signal (see Fig. 5B) implies that the configuration of Q_A is probably dependent on the existence of the quinone molecule at the Q_B position in the reaction center. For the two types of $Q_A^{-\bullet}$ described above, we suggest that the high potential form of Q_A with a strong hydrogen-bond can be converted to the low potential form with a weak hydrogen-bond after the recovery of the Q_B occupation in intact PSII. This relationship between Q_A configuration and the occupation of Q_B would have an important physiological function as the occupation of Q_B is changeable *in vivo*. The Q_B position can be either occupied or empty under physiological condition. When the Q_B position is empty, charge recombination would be ready to take place and lead to the formation of triplet Chl a at the donor site. The triplet Chl a is able to react with triplet oxygen to produce aggressive singlet oxygen [74,75]. Moreover, the negative charge on Q_A is also ready to react with an oxygen molecule to form superoxide radical ($O_2^{-\bullet}$) at the acceptor site [76]. Both $^1O_2$ and $O_2^{-\bullet}$ are extremely harmful species to PSII [74,75]. Therefore, it is crucial to stabilize the electron on Q_A. The strong hydrogen-bond between $Q_A^{-\bullet}$ and His_{214} could be a strategy to stabilize the negative charge and prevent charge recombination, thus diminishing the possibility of $^1O_2$ and $O_2^{-\bullet}$ formation. On the other hand, the weak hydrogen-bond between Q_A and His_{214} could contribute to promoting electron transfer between Q_A and Q_B when functional Q_B is present.

4.3. Implications for electron transfer at cryogenic temperatures

The oxidation of both Tyr_Z and the side-path electron donors have been observed at low temperature in intact PSII recently. The oxidation reactions of Car/Chl_Z and Cyt_{b559} only involve electron transfer, and their oxidations at low temperature have been observed in both intact and inhibited samples [30,31,33-36,77-81]. In contrast, the oxidation of Tyr_Z is accompanied by proton release from the phenolic oxygen [17,18], and efficient Tyr_Z oxidation at liquid helium temperature has only been observed in the S_0 and S_1 states in intact PSII [21,38,40]. It has been suggested that the oxidation of Tyr_Z can only occur when the hydrogen bond between Tyr_Z and His_{190} is strong so that proton movement is possible even at liquid helium temperatures [38,42]. Thus, the static heterogeneity of the Tyr_Z at the donor side would certainly affect the low-temperature electron transfer as discussed in previous reports [38,42,46].

It is noted that, in most previous reports, the reason for the selection of the low-temperature electron transfer has been only considered in the aspect of the donor side (see [34,38,42] for example). We have recently found that the redox potential of the non-heme iron and the existence of Q_B at the acceptor site significantly affect the oxidation of these secondary electron donors in intact PSII [46]. In the previous report, we suggested that the electrostatic effect and/or possible structural cooperation between the acceptor and donor sites could contribute to oxidation selection of these secondary electron donors at low temperature. However, as the non-heme iron and Q_B are not directly involved in low-temperature electron transfer, the unambiguous answer for the mode of selection of electron transport pathway is still unknown. Our present experiments clearly point to two types of Q_A in intact PSII. One is associated with the oxidation of the side-path electron donors; the other is associated with Tyr_Z oxidation at low temperatures. However, an unambiguous conclusion on whether the mode of selection of electron transport pathway for the oxidation of Tyr_Z or the side-path electron donors at low temperatures is directly related to any changes of Q_A configuration at the acceptor side, or is due to changes of Tyr_Z simultaneously at the donor side as a result of the changes of Q_A at the acceptor side, are still waiting for further detailed kinetic investigations at low temperatures and in the same intact PSII samples. Nevertheless, our results may shed new insight into the understanding of the mode of selection of electron transport pathway for the oxidation of these secondary electron donors at low temperatures.

5. Conclusion

In this paper, the correlation between the reduction of Q_A and the oxidation of Tyr_Z or $Car/Chl_Z/Cyt_{b559}$ induced by visible light at liquid helium temperatures has been studied using electron paramagnetic resonance. Our results indicate that two types of Q_A may exist in intact spinach PSII. The EPR-detectable $g = 1.95–1.86$ $Q_A^{-\bullet}$ signal is only correlated with oxidation of the side-path electron donors ($Car/Chl_Z/Cyt_{b559}$), but not of Tyr_Z. The strength of the hydrogen-bond between Q_A and D_2-His_{214} bound to the non-heme iron is discussed to explain the difference of Q_A observed at 10 K. It would be interesting to verify if different configurations of Q_A exist at physiological temperatures. It is suggested that the conversion of these two types of $Q_A^{-\bullet}$ may have an important physiological effect by promoting electron transfer from Q_A to Q_B, and preventing the formation of harmful species ($^1O_2$ and $O_2^{-\bullet}$) *in vivo*.

Acknowledgments

This work was supported by the Chinese Academy of Sciences and the National Natural Science Foundation of China with No. 20403024, 30570423, 20973186. CZ would like to thank Prof. Yandao Gong for help with the oxygen evolution measurement, and thanks to Dr. Jie Pan for carefully reading the manuscript and making valuable comments on it.

References

[1] C. Goussias, A. Boussac, A.W. Rutherford, Photosystem II and photosynthetic oxidation of water: an overview, Philos. Trans. R. Soc. Lond. B 357 (2002) 1369–1381.
[2] K. Satoh, T.J. Wydrzynski, Govindjee, Introduction to photosystem II, in: T.J. Wydrzynski, K. Satoh (Eds.), Photosystem II: The Light-Driven water: Plastoquinone Oxidoreductase, Springer, The Netherlands, 2005, pp. 11–22.
[3] G. Renger, T. Renger, Photosystem II, The machinery of photosynthetic water splitting, Photosynth. Res. 98 (2008) 53–80.
[4] N. Kamiya, J.R. Shen, Crystal structure of oxygen-evolving photosystem II from *Thermosynechococcus vulcanus* at 3.7 Å resolution, Proc. Natl. Acad. Sci. U. S. A. 100 (2003) 98–103.
[5] B. Loll, J. Kern, W. Saenger, A. Zouni, J. Biesiadka, Towards complete cofactor arrangement in the 3.0Å resolution structure of photosystem II, Nature 438 (2005) 1040–1044.
[6] K.N. Ferreira, T.M. Iverson, K. Maghlaoui, J. Barber, S. Iwata, Architecture of the photosynthetic oxygen-evolving center, Science 303 (2004) 1831–1838.
[7] A. Guskov, J. Kern, A. Gabdulkhakov, M. Broser, A. Zouni, W. Saenger, Cyanobacterial photosystem II at 2.9-Å resolution and the role of quinones, lipids, channels and chloride, Nat. Struct. Mol. Biol. 16 (2009) 334–342.
[8] K. Kawakami, Y. Umena, N. Kamiya, J.R. Shen, Location of chloride and its possible functions in oxygen-evolving photosystem II revealed by X-ray crystallography, Proc. Nat. Acad. Sci. U. S. A. 106 (2009) 8567–8572.
[9] A. Zouni, H.T. Witt, J. Kern, P. Fromme, N. Kraub, W. Saenger, P. Orth, Crystal structure of photosystem II from *Synechococcus elongatus* at 3.8 Å resolution, Nature 409 (2001) 739–743.

[10] G. Renger, A.R. Holzwarth, Primary electron transfer, in: T.J. Wydrzynski, K. Satoh (Eds.), Photosystem II: The Light-Driven water: Plastoquinone Oxidoreductase, Springer, The Netherlands, 2005, pp. 139–175.
[11] N. Nelson, C.F. Yocum, Structure and function of photosystem I and II, Ann. Rev. Plant Biol. 57 (2006) 521–565.
[12] B.A. Diner, F. Rappaport, Structure, dynamics, and energetics of the primary photochemistry of photosystem II of oxygenic photosynthesis, Ann. Rev. Plant Biol. 53 (2002) 551–580.
[13] G. Renger, P. Kühn, Reaction pattern and mechanism of light induced oxidative water splitting in photosynthesis, Biochim. Biophys. Acta 1767 (2007) 471–485.
[14] F. Rappaport, B.A. Diner, Primary photochemistry and energetics leading to the oxidation of the (Mn)4Ca cluster and to the evolution of molecular oxygen in Photosystem II, Coor. Chem. Rev. 252 (2008) 259–272.
[15] V. Petrouleas, A.R. Crofts, The iron-quinone acceptor complex, in: T.J. Wydrzynski, K. Satoh (Eds.), Photosystem II: The Light-Driven water: Plastoquinone Oxidoreductase, Springer, The Netherlands, 2005, pp. 177–206.
[16] B.A. Diner, V. Petrouleas, J.J. Wendoloski, The iron–quinone electron–acceptor complex of photosystem II, Physiol. Plant. 81 (1991) 423–436.
[17] G.T. Babcock, B.A. Barry, R.J. Debus, C.W. Hoganson, M. Atamian, L. McIntosh, I. Sithole, C.F. Yocum, Water oxidation in photosystem 2 from radical chemistry to multielectron chemistry, Biochemistry 28 (1989) 9557–9565.
[18] B.A. Diner, R.D. Britt, The redox-active tyrosines Y_Z and Y_D, in: T.J. Wydrzynski, K. Satoh (Eds.), Photosystem II: The Light-Driven water: Plastoquinone Oxidoreductase, Springer, The Netherlands, 2005, pp. 207–233.
[19] R.J. Debus, The manganese and calcium-ions of photosynthetic oxygen evolution, Biochim. Biophys. Acta 1102 (1992) 269–352.
[20] J.P. McEvoy, G.W. Brudvig, Water-splitting chemistry of photosystem II, Chem. Rev. 106 (2006) 4455–4483.
[21] C. Zhang, Low-barrier hydrogen bond plays key role in active photosystem II- a new model for photosynthetic water oxidation, Biochim. Biophys. Acta 1767 (2007) 493–499.
[22] H. Dau, M. Haumann, The manganese complex of photosystem II in its reaction cycle—Basic framework and possible realization at the atomic level, Coord. Chem. Rev. 252 (2008) 273–295.
[23] W. Hillier, J. Messinger, Mechanism of photosynthetic oxygen production, in: T.J. Wydrzynski, K. Satoh (Eds.), Photosystem II: The Light-Driven water: Plastoquinone Oxidoreductase, Springer, The Netherlands, 2005, pp. 567–608.
[24] K.A. Åhrling, R.J. Pace, M.C.W. Evans, The catalytic manganese cluster: implications from spectroscopy, in: T.J. Wydrzynski, K. Satoh (Eds.), Photosystem II: The Light-Driven water: Plastoquinone Oxidoreductase, Springer, The Netherlands, 2005, pp. 285–306.
[25] V.I. Prokhorenko, A.R. Holzwarth, Primary processes and structure of the photosystem II reaction center: a photon echo study, J. Phys. Chem. B 104 (2000) 11563–11578.
[26] F.v. Mieghem, K. Brettel, B. Hillmann, A. Kamlowski, A.W. Rutherford, E. Schlodder, Charge recombination reactions in photosystem II. 1. Yields, recombination pathways, and kinetics of the primary pair, Biochemistry 34 (1995) 4798–4813.
[27] A. Garbers, F. Reifarth, J. Kurreck, G. Renger, F. Parak, Correlation between protein flexibility and electron transfer from Q_A^- to Q_B in PSII membrane fragments from spinach, Biochemistry 37 (1998) 11399–11404.
[28] F. Reifarth, G. Renger, Indirect evidence for structural changes coupled with Q_B^- formationin photosystem II, FEBS Lett. 428 (1998) 123–126.
[29] C. Fufezan, C. Zhang, A. Krieger-Liszkay, A.W. Rutherford, Secondary quinone in photosystem II of *Thermosynechococcus elongatus*: Semiquinone-iron EPR signals and temperature dependence of electron transfer, Biochemistry 44 (2005) 12780–12789.
[30] B. Hillmann, E. Schlodder, Electron transfer reactions in photosystem II core complexes from *Synechcoccus* at low temperature-difference spectrum of $P_{680}^+Q_A^-$/$P_{680}Q_A$ at 77K, Biochim. Biophys. Acta 1231 (1995) 76–88.
[31] D.H. Stewart, G.W. Brudvig, Cytochrome b559 of photosystem II, Biochim. Biophys. Acta 1367 (1998) 63–87.
[32] P. Faller, A. Pascal, A.W. Rutherford, b-Carotene redox reactions in photosystem II: electron transfer pathway, Biochemistry 40 (2001) 6431–6440.
[33] C.A. Tracewell, A. Cua, D.H. Stewart, D.F. Bocian, G.W. Brudvig, Characterization of carotenoid and chlorophyll photooxidation in photosystem II, Biochemistry 40 (2001) 193–203.
[34] P. Faller, C. Fufezan, A.W. Rutherford, Side-path electron donors: cytochrome b559, chlorophyll $_Z$ and b-carotene, in: T.J. Wydrzynski, K. Satoh (Eds.), Photosystem II: The Light-Driven water: Plastoquinone Oxidoreductase, Springer, The Netherland, 2005, pp. 347–365.
[35] C.A. Tracewell, G.W. Brudvig, Multiple redox-active chlorophylls in the secondary electron-transfer pathways of oxygen-evolving photosystem II, Biochemistry 47 (2008) 11559–11572.
[36] J.L. Hughes, A.W. Rutherford, M. Sugiura, E. Krausz, Quantum efficiency distributions of photo-induced side-pathway donor oxidation at cryogenic temperature in photosystem II, Photosynth. Res. 98 (2008) 199–206.
[37] D. Koulougliotis, C. Teutloff, Y. Sanakis, W. Lubitz, V. Petrouleas, The $S_1Y_Z^{\bullet}$ metalloradical intermediate in photosystem II: an X-and W-band EPR study, Phys. Chem. Chem. Phys. 6 (2004) 4859–4863.
[38] C. Zhang, S. Styring, Formation of split electron paramagnetic resonance signals in photosystem II suggests that tyrosine$_z$ can be photooxidized at 5 K in the S_0 and S_1 states of the oxygen-evolving complex, Biochemistry 42 (2003) 8066–8076.
[39] J.H.A. Nugent, I.P. Muhiuddin, M.C.W. Evans, Electron transfer from the water oxidizing complex at cryogenic temperatures: the S_1 to S_2 step, Biochemistry 41 (2002) 4117–4126.
[40] C. Zhang, A. Boussac, A.W. Rutherford, Low-temperature electron transfer in photosystem II: A tyrosyl radical and semiquinone charge pair, Biochemistry 43 (2004) 13787–13795.
[41] D. Koulougliotis, J.R. Shen, N. Ioannidis, V. Petrouleas, Near-IR irradiation of the S_2 state of the water oxidizing complex of photosystem II at liquid helium temperatures produces the metalloradical intermediate attributed to $S_1Y_Z^{\bullet}$, Biochemistry 42 (2003) 3045–3053.
[42] V. Petrouleas, D. Koulougliotis, N. Ioannidis, Trapping of metalloradical intermediates of the S-states at liquid helium temperatures. Overview of the phenomenology and mechanistic implications, Biochemistry 44 (2005) 6723–6728.
[43] A. Boussac, M. Sugiura, T.L. Lai, A.W. Rutherford, Low-temperature photochemistry in photosystem II from *Thermosynechococcus elongatus* induced by visible and near-infrared light, Phil. Trans. R. Soc. B 363 (2008) 1203–1210.
[44] G. Han, F.M. Ho, K.G.V. Havelius, S.F. Morvaridi, F. Mamedov, S. Styring, Direct quantification of the four individual S states in Photosystem II using EPR spectroscopy, Biochim. Biophys. Acta 1777 (2008) 496–503.
[45] N. Ioannidis, G. Zahariou, V. Petrouleas, The EPR spectrum of tyrosine $Z^{\bullet}$ and its decay kinetics in O_2-evolving photosystem II preparations, Biochemistry 47 (2008) 6292–6300.
[46] H. Bao, C. Zhang, K. Kawakami, Y. Ren, J.R. Shen, J. Zhao, Acceptor side effects on the electron transfer at cryogenic temperatures in intact photosystem II, Biochim. Biophys. Acta 1777 (2008) 1109–1115.
[47] A.E. McDermott, V.K. Yachandra, R.D. uiles, J.L. Cole, S.L. Dexheimer, R.D. Britt, K. Sauer, M.P. Klein, Characterization of the manganese oxygen-evolving complex and the iron-quinone acceptor complex in photosystem II from a thermophilic cyanobacterium by electron paramagnetic resonance and X-ray absorption spectroscopy, Biochemistry 27 (1988) 4021–4031.
[48] J.H.A. Nugent, B.A. Diner, M.C.W. Evans, Direct detection of the electron acceptor of photosystem II, FEBS Lett. 124 (1981) 241–244.
[49] A.W. Rutherford, J.L. Zimmermann, A new EPR signal attributed to the primary plastosemiquinone acceptor in photosystem II, Biochim. Biophys. Acta 767 (1984) 168–175.
[50] W.F.J. Vermaas, A.W. Rutherford, EPR measurements on the effects of bicarbonate and triazine resistance on the acceptor side of Photosystem II, FEBS Lett. 175 (1984) 243–248.
[51] C.H. Goussias, Y. Deligiannakis, Y. Sanakis, N. Ioannidis, V. Petrouleas, Probing subtle coordination changes in the iron–quinone complex of photosystem II during electron transfer, by the use of NO, Biochemistry 41 (2002) 15212–15223.
[52] A.R. Corrie, J.H.A. Nugent, M.C.W. Evans, Identification of EPR signals from the states $Q_A^-Q_B$and Q_B^-in photosystem II from *Phormidium laminosum*, Biochim. Biophys. Acta 1057 (1991) 384–390.
[53] F. MacMillan, F. Lendzian, G. Renger, W. Lubitz, EPR and ENDOR Investigation of the primary electron acceptor radical anion Q_A^- in iron-depleted photosystem II membrane fragments, Biochemistry 34 (1995) 8144–8156.
[54] D.A. Berthold, G.T. Babcock, C.F. Yocum, A highly resolved, oxygen-evolving photosystemII , preparation from spinach thylakoid membranes, FEBS Lett. 134 (1981) 231–234.
[55] Y. Ren, C. Zhang, H. Bao, J. Shen, J. Zhao, Probing tyrosine$_Z$ oxidation in photosystem II core complex isolated from spinach by EPR at liquid helium temperatures, Photosynth. Res. 99 (2009) 127–138.
[56] C. Zhang, Interaction between tyrosine$_Z$ and substrate water in active photosystem II, Biochim. Biophys. Acta 1757 (2006) 781–786.
[57] H. Kuhne, G.W. Brudvig, Proton-coupled electron transfer involving tyrosine Z in photosystem II, J. Phys. Chem. B 106 (2002) 8189–8196.
[58] P. Faller, A.W. Rutherford, R.J. Debus, Tyrosine D oxidation at cryogenic temperature in photosystem II, Biochemistry 41 (2002) 12914–12920.
[59] J.H. Su, K.G.V. Havelius, F. Mamedov, F.M. Ho, S. Styring, Split EPR signals from photosystem II are modified by methanol, reflecting S state-dependent binding and alterations in the magnetic coupling in the $CaMn_4$ cluster, Biochemistry 45 (2006) 7617–7627.
[60] J.H.A. Nugent, I.P. Muhiuddin, M.C.W. Evans, Effect of hydroxylamine on photosystem II: reinvestigation of electron paramagnetic resonance characteristics reveals possible S state intermediates, Biochemistry 42 (2003) 5500–5507.
[61] J.L. Zimmermann, A.W. Rutherford, Photoreduction-induced oxidation of Fe^{2+}in the electron-acceptor complex of photosystem II, Biochim. Biophys. Acta 851 (1986) 416–423.
[62] U. Heinen, L.M. Utschig, O.G. Poluektov, G. Link, E. Ohmes, G. Kothe, Structure of the charge separated state $P_{865}^+Q_A^-$ in the photosynthetic reaction centers of *Rhodobacter sphaeroides* by quantum beat oscillations and high-field electron paramagnetic resonance: Evidence for light-induced Q_A^- reorientation, J. Am. Chem. Soc. 129 (2007) 15935–15946.
[63] F. Rappaport, A. Cuni, L. Xiong, R. Sayre, J. Lavergne, Charge recombination and thermoluminescence in photosystem II, Biophys. J. 88 (2005) 1948–1958.
[64] W.F. Butler, R. Calvo, D.R. Fredkin, R.A. Isaacson, M.Y. Okamura, G. Feher, The electronic structure of Fe^{2+}in reaction centers from *Rhodopseduomonas sphaeroides* III. EPR measurements of the reduced acceptor complex, Biophys. J. 45 (1984) 947–973.
[65] G.C. Dismukes, H.A. Frank, R. Friesner, K. Sauer, Electronic interactions between iron and the bound semiquinones in bacterial photosynthesis. EPR spectroscopy of oriented cells of *Rhodopseudomonas viridis*, Biochim. Biophys. Acta 764 (1984) 253–271.
[66] P.W. Anderson, P.R. Weiss, Exchange narrowing in paramagnetic resonance, Rev. Mod. Phys. 25 (1953) 269–276.
[67] C. Berthomieu, E. Nabedryk, W. Mäntele, J. Breton, Characterization by FTIR difference spectroscopy of the photoreduction of the primary quinone acceptor Q_A in photosystem II, FEBS Lett. 269 (1990) 363–367.

[68] T. Noguchi, Y. Inoue, X.S. Tang, Hydrogen bonding interaction between the primary quinone acceptor Q_A and a histidine side chain in photosystem II as revealed by Fourier transform infrared spectroscopy, Biochemistry 38 (1999) 399–403.
[69] T. Noguchi, J. Kurreck, Y. Inoue, G. Renger, Comparative FTIR analysis of the microenvironment of $Q_A^{-\cdot}$ in cyanide-treated, high pH-treated and iron-depleted photosystem II membrane fragments, Biochemistry 38 (1999) 4846–4852.
[70] J. Yano, J. Kern, K.D. Irrgang, M.J. Latimer, U. Bergmann, P. Glatzel, Y. Pushkar, J. Biesiadka, B. Loll, K. Sauer, J. Messinger, A. Zouni, V.K. Yachandra, X-ray damage to the Mn_4Ca complex in single crystals of photosystem II: a case study for metalloprotein crystallography, Proc. Nat. Acad. Sci. U. S. A. 102 (2005) 12047–12052.
[71] M. Grabolle, M. Haumann, C. Müller, P. Liebisch, H. Dau, Rapid loss of structural motifs in the manganese complex of oxygenic photosynthesis by X-ray irradiation at 10-300K, J. Biol. Chem. 281 (2006) 4580–4588.
[72] L.M. Utschig, S.D. Chemerisov, D.M. Tiede, O.G. Poluektov, Electron paramagnetic resonance study of radiation damage in photosynthetic reaction center crystals, Biochemistry 47 (2008) 9251–9257.
[73] G.N. Johnson, A.W. Rutherford, K. Krieger, A change in the midpoint potential of the quinone Q_A in photosystem II associated with photoactivation of oxygen evolution, Biochim Biophys. Acta 1229 (1995) 202–207.
[74] A.W. Rutherford, A. Krieger-Liszkay, Herbicide-induced oxidative stress in photosystem II, Trends Biochem. Sci. 26 (2001) 648–653.
[75] A. Krieger-Liszkay, C. Fufezan, A. Trebst, Singlet oxygen production in photosystem II and related protection mechanism, Photosynth. Res. 98 (2008) 551–564.
[76] P. Pospíšil, A. Arató, A. Krieger-Liszkay, A.W. Rutherford, Hydroxyl radical generation by photosystem II, Biochemistry 43 (2004) 6783–6792.
[77] P. Mathis, A. Vermeglio, Chlorophyll radical cation in photosystem II of chloroplasts. Millisecond decay at low temperature, Biochim, Biophys. Acta 396 (1975) 371–381.
[78] J. Hanley, Y. Deligiannakis, A. Pascal, P. Faller, A.W. Rutherford, Carotenoid oxidation in photosystem II, Biochemistry 38 (1999) 8189–8195.
[79] P. Faller, T. Maly, A.W. Rutherford, F. MacMillan, Chlorophyll and carotenoid radicals in photosystem II studied by pulsed ENDOR, Biochemistry 40 (2001) 320–326.
[80] J.L. Hughes, P. Smith, R. Pace, E. Krausz, Charge separation in photosystem II core complexes induced by 690–730 nm excitation at 1.7 K, Biochim. Biophys. Acta 1757 (2006) 841–851.
[81] T. Noguchi, T. Mitsuka, Y. Inoue, Fourier-transform infrared spectrum of the radical cation of β-carotene photoinduced in photosystem II, FEBS Lett. 356 (1994) 179–182.